
This is the accepted manuscript version of the article

Role of calcium on chloride binding in hydrated Portland cement–metakaolin–limestone blends

Shi, Z., Geiker, M. R., De Weerd, K., Østnor, T. A., Lothenbach, B., Winnefeld, F., & Skibsted, J.

Citation for the published version (APA 6th)

Shi, Z., Geiker, M. R., De Weerd, K., Østnor, T. A., Lothenbach, B., Winnefeld, F., & Skibsted, J. (2017). Role of calcium on chloride binding in hydrated Portland cement–metakaolin–limestone blends. *Cement and Concrete Research*, 95(Supplement C), 205-216.
doi:<https://doi.org/10.1016/j.cemconres.2017.02.003>

This is accepted manuscript version.

It may contain differences from the journal's pdf version.

This file was downloaded from SINTEFs Open Archive, the institutional repository at SINTEF
<http://brage.bibsys.no/sintef>

1 **Role of calcium on chloride binding in hydrated Portland**
2 **cement – metakaolin – limestone blends**

3
4 Zhenguo Shi^a, Mette Rica Geiker^b, Klaartje De Weerd^{b,c}, Tone Anita Østnor^c,
5 Barbara Lothenbach^d, Frank Winnefeld^d, Jørgen Skibsted^{a*}

6
7 a. Department of Chemistry and Interdisciplinary Nanoscience Center (iNANO), Aarhus
8 University, DK-8000 Aarhus C, Denmark

9 b. Department of Structural Engineering, Norwegian University of Science and Technology
10 (NTNU), 7491 Trondheim, Norway

11 c. SINTEF Building and Infrastructure, 7491 Trondheim, Norway

12 d. Laboratory for Concrete & Construction Chemistry, Swiss Federal Laboratories for
13 Materials Science and Technology (Empa), 8600 Dübendorf, Switzerland

14
15
16
17
18
19
20
21
22
23
24
25
26 _____

27 * Corresponding author. Department of Chemistry and Interdisciplinary Nanoscience Center
28 (iNANO), Aarhus University, DK-8000 Aarhus C, Denmark. Tel: +45-8715 5946; Fax: +45
29 8619 6199. E-mail address: jskib@chem.au.dk (J. Skibsted).

32 **Abstract**

33 Chloride binding is investigated for Portland cement – metakaolin – limestone pastes exposed
34 to CaCl_2 and NaCl solutions. The phase assemblages and the amount of Friedel’s salt are
35 evaluated using TGA, XRD and thermodynamic modeling. A larger amount of Friedel’s salt is
36 observed in the metakaolin blends compared to the pure Portland cement. A higher total
37 chloride binding is observed for the pastes exposed to the CaCl_2 solution relative to those in the
38 NaCl solution. This is reflected by the fact that calcium increases the quantity of Friedel’s salt
39 in the metakaolin blends by promoting the transformation of strätlingite and/or monocarbonate
40 to Friedel’s salt. Calcium increases also the amount of chloride in the diffuse layer of the C-S-
41 H for the pure cement. A linear correlation between the total bound chloride and the uptake of
42 calcium from the CaCl_2 solution is obtained and found to be independent on the type of cement
43 blend.

44

45

46 **Keywords:** Chloride (D); Metakaolin (D); pH (A); Calcium-Silicate-Hydrate (C-S-H) (B);

47 Thermodynamic Calculations (B).

48

49

50 **1 Introduction**

51 Corrosion of steel reinforcement leads to loss of structural integrity and serviceability of
52 reinforced concrete. An important contribution to this degradation is penetration of chloride
53 ions from de-icing salt or sea water into reinforced concrete, which results in depassivation of
54 the steel reinforcement when the chloride concentration exceeds a certain threshold level [1].
55 Attention to this problem has been paid for more than fifty years, during which significant
56 research efforts have been made and several reviews have been published on this issue [2-5].
57 According to published studies, chloride ions in chloride exposed concrete are chemically
58 bound in Friedel's salt ($\text{Ca}_4\text{Al}_2(\text{OH})_{12}\text{Cl}_2 \cdot 4\text{H}_2\text{O}$) or present in the diffuse layer of the calcium-
59 silicate-hydrate (C-S-H) phase, where both forms are often referred to as bound chloride. The
60 remaining chloride ions are present in the pore solution, *i.e.*, as free chloride. One of the
61 commonly used methods to evaluate the chloride resistance of concrete is to determine its
62 chloride diffusion coefficient based on the total chloride profiles (*i.e.*, the total chloride content
63 as function of the ingress depth), which is mainly affected by the pore structure [6, 7]. In
64 addition to physical restrictions, several studies have also stated that chloride binding by the
65 hydrated cement in concrete may affect the rate of chloride ingress [2, 8-11]. However, a recent
66 study [12] has strongly indicated that chloride ions pass easily through the diffusion layer of
67 the C-S-H. These findings from the literature underline the needs to further improve our
68 knowledge on the different chloride binding mechanisms in order to assess the chloride
69 resistance of concrete.

70 An efficient approach to enhance the chloride binding capacity of concrete is to partially
71 replace Portland cement by alumina-rich supplementary cementitious materials (SCMs) [13-
72 18], which are also beneficial for improvement of the pore structure [15, 19] and strength
73 enhancement [19, 20] when an optimized replacement level is used. Heat-treated clay minerals
74 represent a promising source of SCMs, as they are rich in alumina and silica. Furthermore,
75 calcined clays receive increasing research interest because of their lower carbon footprint as
76 compared to Portland cement and high abundance in the Earth's crust which make them
77 attractive alternatives to industrial byproducts such as fly ash and slag. Limestone represents
78 another type of SCM which is found to generate a synergetic effect with alumina-rich SCMs in
79 blended Portland cements [21, 22]. The presence of such synergetic effects promotes the
80 combined utilization of calcined clays (*e.g.* metakaolin) and limestone to replace Portland
81 cement at high replacement levels without sacrificing the compressive strength of the resulting
82 concrete [23, 24]. Significant research efforts have been devoted to the development and
83 characterization of Portland cement – calcined clay – limestone blends, as recently summarized

84 in ref. [25]. The present work focuses on the chloride binding in Portland cement – metakaolin
85 – limestone blends. A series of other durability investigations, *i.e.*, chloride ingress,
86 carbonation and resistance to sulfate attack, have recently been presented for very similar
87 blends [7, 26, 27].

88 The main contribution of alumina-rich SCMs on chloride binding is generally believed to be
89 related to the alumina content of the mixture through formation of Friedel’s salt. Very few
90 studies focus on the chloride adsorption in the diffuse layer of the C-S-H phase in these blends,
91 even though evidence for physical chloride binding on the surface of the C-S-H phase has been
92 reported in several studies for synthetic C-S-H phases [28-30], hydrated Ca_3SiO_5 (C_3S) [31, 32],
93 Portland cement [33], and silica fume – lime blends [34]. Because of the variations in
94 composition and structure of the C-S-H phase, the physical chloride binding in the diffuse layer
95 on the surface of the C-S-H becomes more complicated, which prevents the development of a
96 reliable approach to evaluate its contribution to the measured total chloride binding, particular
97 in blends with alumina-rich SCMs.

98 Several studies have also reported that the associated cations (*e.g.* Ca^{2+}) have a significant
99 influence on chloride binding [17, 30, 32, 35-40]. A consistent conclusion from these
100 investigations is that a higher total chloride binding is observed for samples exposed to CaCl_2
101 solutions as compared to NaCl solutions of the same chloride-ion concentration. The chloride
102 binding has also been observed to increase with decreasing pH of the CaCl_2 exposure solutions
103 with increasing chloride-ion concentration [32, 36, 37, 40, 41]. A linear relationship between
104 the pH of the exposure solution (*i.e.*, for solutions of MgCl_2 , CaCl_2 and NaCl) and the chloride
105 binding has been established which is found to be independent of type of salt [37]. Based on
106 this observation, it was concluded that the impact of different cations on the chloride binding is
107 mainly governed by the pH of the exposure solution. However, it should be noted that these
108 studies generally focused on synthetic C-S-H samples, hydrated C_3S and Portland cements
109 whereas only a very few investigations have considered this effect for blends of Portland
110 cement with SCMs. Thus, the conclusions, in particular for the pH dependency of the chloride
111 binding, need to be verified for systems including SCMs. Furthermore, the driving force of the
112 pH change on chloride binding should be analyzed in more detail to achieve a better
113 understanding of the mechanisms of chloride binding.

114 The aim of this work is to investigate the impact of cations, Ca^{2+} vs. Na^+ , on chloride binding
115 in Portland cement – metakaolin – limestone blends. The total chloride binding isotherms are
116 determined in order to evaluate the total chloride binding capacity of different blends exposed
117 to NaCl and CaCl_2 solutions. The chloride binding in Friedel’s salt is examined by data from

118 thermodynamic modeling and quantitative X-ray diffraction. The amount of chloride
119 associated with the C-S-H phase is calculated by subtracting the amount of bound chloride in
120 Friedel's salt from the total bound chloride determined by an equilibrium approach. The phase
121 assemblages are analyzed by thermogravimetric analysis, X-ray diffraction and thermodynamic
122 modelling. The pH values as well as the concentrations of chloride and calcium ions in the
123 exposure solution are also determined. Based on these investigations, the role of calcium on
124 chloride binding is assessed for Portland cement – metakaolin – limestone blends.

125

126 **2 Experimental**

127 The experimental setup, including preparation of the pastes, the exposure experiments and the
128 analysis of the solids and solutions for obtaining the chloride binding isotherms, follows
129 procedures described recently [37, 41].

130

131 **2.1 Materials**

132 The binders used in this study were made from a white Portland cement (wPc, CEM I 52.5 N),
133 metakaolin (MK) and limestone (LS). The wPc was produced by Aalborg Portland A/S,
134 Denmark, and included 3.1 wt.% LS, 4.1 wt.% gypsum and 1.9 % wt.% free lime. The MK
135 was produced in the laboratory from kaolinite (Kaolinite SupremeTM, Imerys Performance
136 Minerals, UK) by thermal treatment in air at 550 °C for 20 h. The LS was a Maastrichtian
137 chalk from Rørdal, Northern Denmark. The chemical compositions determined by X-ray
138 fluorescence (XRF), the density and Blaine fineness for the starting materials are given in
139 [Table 1](#). The wPc contained 64.9 wt.% alite (“3CaO·SiO₂”: C₃S), 16.9 wt.% belite
140 (“2CaO·SiO₂”: C₂S) and 7.8 wt.% calcium aluminate (3CaO·Al₂O₃: C₃A). The content of the
141 silicate phases were determined by ²⁹Si MAS NMR, assuming the Taylor compositions for
142 these phases [42] and the quantity of the calcium aluminate phase by subsequent mass balance
143 calculations. The small amount of iron is expected to be incorporated as guest ions in the alite,
144 belite and C₃A phases. The salts, NaCl and CaCl₂·6H₂O, of laboratory grade were dissolved in
145 distilled water to prepare exposure solutions with the following chloride-ion concentrations: 0
146 (reference), 0.125, 0.25, 0.50, 1.0 and 2.0 mol/L. The actual concentrations were checked by
147 titration prior to use.

148

149 **2.2 Preparation of cement pastes**

150 The binder compositions ([Table 2](#)) are the same as those used for mortars for carbonation
151 experiments in another study [26]. The degrees of hydration for alite, belite and MK in

152 corresponding paste samples, measured by ^{29}Si MAS NMR, are summarized in Table 3 [43].
153 Three types of pastes (P, ML and M) as listed in Table 2 have been produced with the same
154 water/binder ratio ($w/b = 0.5$) by mass. For each paste, deionized water was added to the
155 cement blend and the paste was mixed (100 g blended cement + 50 g water for each mixing) by
156 a motorized stirrer (Heidolph® RZR-2, Germany) equipped with a custom-made paddle (\varnothing 45
157 mm). The mixing employed a rotational speed of 500 rpm for 3 minutes, then no rotation for 2
158 minutes, followed by mixing at 2000 rpm for 2 minutes, and the blend was then cast and sealed
159 in a plastic bag. The fresh paste in the bags was flattened to a thickness of about 5 mm to
160 facilitate the release of heat during hydration and avoid formation of hydration shells around
161 the hydrating cement grains in order to maximize the degree of hydration [44]. For the same
162 purpose of releasing heat during initial hydration, the pastes were sealed cured in a moist
163 cabinet at 5 °C for the first three days followed by an additional curing in a moist room with
164 relative humidity higher than 98% at 20 °C for about 2 months. Then the cement paste plates
165 were crushed in a ceramic mortar to particles with a diameter of approximately 1 mm. The
166 resulting powder was collected then in a one-liter polypropylene bottle and mixed with distilled
167 water (30 % by mass of the powdered cement paste). The new mixes with a resulting w/b of
168 0.95 were stored in bottles and rotated slowly along the longitudinal axis for additional 7 days
169 at 20 °C. Each moist cement paste was crushed and homogenized with a stainless steel bar,
170 resulting in a sample with the appearance as “moist sand”. This procedure for preparation of
171 the pastes aims to maximize the degree of hydration of the cement pastes and minimize
172 possible carbonation prior to chloride exposure [37, 41]. Moreover, a possible minor degree of
173 bleeding for the freshly prepared pastes ($w/b = 0.50$) may only give minor contribution to
174 heterogeneity in the samples as they have been ground and rehydrated with additional water
175 after 2 months of hydration.

176

177 **2.3 Chloride exposure**

178 The well-hydrated pastes were exposed to the chloride solutions by the following procedure:
179 30.0 g of the hydrated cement paste ($w/b = 0.95$) was weighed into a 45 mL plastic centrifuge
180 tube and 15.0 mL of the chloride solution was added. A reference sample exposed to the same
181 amount of distilled water was also prepared. The samples were sealed, stored in the plastic
182 centrifuge tubes at 20 °C for 2 months and shaken regularly prior to analysis. The samples were
183 prepared with different numbers of replicates (one reference sample for distilled water, two
184 samples for the 0.125, 0.25, and 2.0 mol/L chloride-ion solutions, and three samples for the
185 0.50 and 1.0 mol/L chloride-ion concentrations).

186

187 2.4 Methods

188 2.4.1 Thermodynamic modeling

189 Thermodynamic modeling was carried out using the Gibbs free energy minimization software
190 GEMS 3.3 [45, 46], which calculates the equilibrium phase assemblages in chemical systems
191 from their total bulk elemental composition. The default databases were expanded with the
192 CEMDATA14 database [45, 46] including solubility products of the solids relevant for
193 cementitious materials. For the C-S-H phase, the CSHQ model proposed by Kulik [47] was
194 used.

195 The changes in phase assemblages upon exposure to the chloride solutions were predicted for
196 the different blends. The phase compositions of the chloride-free blends after hydration for 91
197 days (> 70 days of sample preparation) were calculated using the degrees of hydration for alite,
198 belite, and metakaolin, as determined by ^{29}Si MAS NMR [43] (*c.f.*, Table 3). These data
199 indicate that only a minor increase in the degree of hydration takes place during the chloride
200 exposure; full hydration is assumed for the calcium aluminate phase as supported by ^{27}Al MAS
201 NMR [43].

202 The effect of the NaCl and CaCl₂ solutions was modelled for chloride concentrations between
203 0.0 and 2.0 mol/L, employing the same amount of water as in the experiments (*i.e.*, 192.5 g
204 water per 100 g anhydrous cement blend including the mixing water of the pastes). This allows
205 prediction of the progressive change in phases with increasing chloride concentration after
206 reaching an equilibrium condition. The activity coefficients were calculated using the extended
207 Debye–Hückel equation in the Truesdell–Jones form with ion size and extended term
208 parameter for NaCl ($\hat{a} = 3.72 \text{ \AA}$ and $b_{\gamma} = 0.064 \text{ kg/mol}$) [48], which is applicable up to an ionic
209 strength of approx. 1 - 2 mol/L [49]. While at higher ionic strength the use of the Pitzer activity
210 corrections would result in more precise aqueous concentrations, the use of extended Debye–
211 Hückel equation has no significant effect on the amount of solid phases calculated in the
212 system studied. During the calculations, the following simplifications were made:

- 213 (i) The uptake of alkali ions by the C-S-H phase is taken into account by employing an ideal
214 solid-solution model between the C-S-H phase and two hypothetical alkali silicate
215 hydrates, $((\text{KOH})_{2.5}\text{SiO}_2\text{H}_2\text{O})_{0.2}$ and $((\text{NaOH})_{2.5}\text{SiO}_2\text{H}_2\text{O})_{0.2}$ [50], as proposed by Kulik *et*
216 *al.* [51].
- 217 (ii) The uptake of aluminum and sulfur by the C-S-H is taken into account by using the
218 reported Al/Si [43] and S/Si [52] ratios summarized in Table 2. The release of Al from
219 C₃S and C₂S during hydration is also considered in the calculations.

220 (iii) The model for Kuzel's salt and Friedel's salt includes pure Kuzel's salt and Friedel's salt
221 and solid solutions of Friedel's salt with carbonate ($\text{CO}_3\text{-AFm}$) and hydroxide
222 (OH-AFm) [53].

223 (iv) The uptake of chloride ions by the C-S-H is not taken into account. It will be estimated
224 by subtracting the chloride content in Friedel's salt from the total bound chloride.

225

226 **2.4.2 Thermogravimetric analysis**

227 Thermogravimetric analysis (TGA) was performed directly on moist paste samples after two
228 months of chloride exposure. A Mettler Toledo TGA/SDTA 851 instrument was used. About
229 1.0 g of the sample was loaded in a 900 μL alumina crucible and dried at 40 $^\circ\text{C}$ in the TGA
230 chamber purged with N_2 for 4 – 5 h, followed by heating up to 950 $^\circ\text{C}$ at rate 10 $^\circ\text{C}/\text{min}$.
231 Friedel's salt formed in the pastes can be identified by TGA from the second of the two main
232 dehydroxylation peaks for Friedel's salt in the temperature ranges 100 – 150 $^\circ\text{C}$ and 230 – 410
233 $^\circ\text{C}$ after chloride exposure. The two weight-loss regions reflect the release of four water
234 molecules from the interlayer between 100 to 150 $^\circ\text{C}$ and six water from the main layer of the
235 Friedel's salt structure at 230 – 410 $^\circ\text{C}$ [7, 54-56].

236

237 **2.4.3 X-ray diffraction analysis**

238 The samples used for the X-ray diffraction analysis (XRD) are the same as those used for TGA.
239 However, the hydration of the paste samples was stopped by immersing the sample first in 60
240 ml of isopropanol for 15 minutes. After filtration the residues were rinsed first with
241 isopropanol and then with diethyl ether. Subsequently, the pastes were dried at 40 $^\circ\text{C}$ for 5
242 minutes and gently ground by hand in an agate mortar. Preparation for the XRD measurements
243 was performed by backloading. The samples were measured without and with 20% CaF_2 ,
244 which was added as internal standard to quantify the total amount of amorphous and minor
245 crystalline phases. A PANalytical X'Pert Pro MPD diffractometer with $\text{CuK}\alpha_1$ radiation in a θ
246 – 2θ configuration was used. The samples were scanned between 5 – 70 $^\circ$ 2θ with the
247 X'Celerator detector during 60 minutes, applying an incident beam monochromator, a 0.5 $^\circ$
248 divergence slit, a 1 $^\circ$ anti-scattering slit on the incident beam side and a 0.04 rad Soller slit on
249 the diffracted beam side. Rietveld refinements were performed using X'Pert HighScore Plus V.
250 3.0.5 using the crystal structures reported in ref. [57]. The background was fitted manually
251 using base points. The refinement procedure included the scale factors, lattice parameters, peak
252 shape parameters and preferred orientation for Friedel's salt.

253

254 2.4.4 Determination of the chloride binding isotherms

255 The “free water” content of the wet pastes ($w/b=0.95$) has been determined by
256 thermogravimetric analysis (TGA) prior to the chloride exposure. Approximately 1.0 g of the
257 wet paste was dried at 40 °C (and not at 105 °C as used recently [37, 41]) in the TGA chamber
258 purged with N₂ for 4 – 5 h during which the weight of sample stabilized. The measured weight
259 loss at 40 °C (“free water” content) was 30.4 wt.% (P), 29.5 wt.% (ML) and 31.4 wt.% (M) of
260 the initial weight of the corresponding wet pastes. The chloride exposed paste samples stored
261 in the tubes were shaken and subsequently centrifuged after 2 months of chloride exposure.
262 However, it should be kept in mind that centrifuging extraction will not 100% remove the free
263 chloride ions from the pore solution, which will result in slightly higher amount of total bound
264 chloride reported. The pH was measured using a Metrohm 6.0255.100 Profitrode calibrated
265 with buffer solutions at predefined pH of 7.0, 10.0 and 13.0. The chloride concentration of the
266 extracted liquid phase at equilibrium was determined by potentiometric titration with 0.010 M
267 AgNO₃(aq) using a Titrand 905 from Metrohm. A high-resolution Element 2 ICP-MS from
268 Thermo Scientific was used to determine the concentration of calcium in solution. The
269 solutions analyzed by ICP-MS were acidified to obtain a HNO₃ concentration of 0.10 mol/L.
270 The chloride binding isotherms were obtained following recently described calculations [41],
271 which are summarized below. The initial chloride concentration ($C_{Cl,initial}$) is calculated from
272 the chloride concentration of the added solution ($C_{Cl,added}$) as follows:

$$273$$
$$274 C_{Cl,initial} = \frac{C_{Cl,added} \times V_{Cl,added}}{V_{H_2O} + V_{Cl,added}} \quad (1)$$
$$275$$

276 where $V_{Cl,added}$ is 15.0 mL and V_{H_2O} is the volume of “free water” available in 30.0 g of
277 hydrated paste sample which is $30.0 \text{ g} \times 30.4 \text{ wt.\%} = 9.1 \text{ g} \approx 9.1.0 \text{ mL}$ for the P sample and 8.9
278 mL and 9.4 mL for the ML (29.5 wt.% of free water) and M (31.4 wt.% of free water) samples,
279 respectively. The bound chloride content ($C_{Cl,total \text{ bound}}$) is calculated from the measured
280 equilibrium chloride concentration in the liquid phase ($C_{Cl,eq}$) by the relation:

$$281$$
$$282 C_{Cl,total \text{ bound}} = \frac{M_{Cl} \times (C_{Cl,initial} - C_{Cl,eq}) \times (V_{H_2O} + V_{Cl,added}) / 1000}{m_{sample} / (1 + 0.95)} \quad (2)$$
$$283$$

284 with $M_{Cl} = 35.45 \text{ g/mol}$, $m_{sample} = 30.0 \text{ g}$, 0.95 being the w/b ratio of the wet pastes, and
285 $m_{sample} / (1 + 0.95)$ as the amount of unhydrated cement blend needed for producing 30.0 g of

286 the resulting paste. Thus, the bound chloride content is reported as g/g of unhydrated cement
 287 blend. In the present study, the discussion on the chloride binding is based on the general
 288 agreement from published studies that the major phases for binding chloride are Friedel's salt
 289 and the C-S-H. The possible minor uptake of chloride ions by other phases (*e.g.* ettringite and
 290 portlandite etc.), as reported in the literature [58], and possible physical adsorption of chloride
 291 on the positive charged surface of Friedel's salt [58] is considered to be negligible. Thus, the
 292 amount of chloride associated with the C-S-H ($C_{Cl,C-S-H}$) can be estimated from the measured
 293 total bound chloride ($C_{Cl,total}$) by subtraction of the chloride content in Friedel's salt ($C_{Cl,FS}$)
 294 predicted by thermodynamic modeling, *i.e.*,

$$C_{Cl,C-S-H} = C_{Cl,total\ bound} - C_{Cl,FS} \quad (3)$$

298 In addition, the calcium binding isotherm reflecting the uptake of calcium by hydration
 299 products from the $CaCl_2$ solution has also been determined. The initial calcium concentration is
 300 calculated as $C_{Ca,initial} = C_{Cl,initial} / 2$ based on the charge balance. The bound calcium
 301 ($C_{Ca,bound}$) is calculated from the measured equilibrium calcium concentration ($C_{Ca,eq}$) and the
 302 initial calcium concentration ($C_{Ca,initial}$) in the liquid phase according to Eq. (4):

$$C_{Ca,bound} = \frac{M_{Ca} \times (C_{Ca,initial} - C_{Ca,eq}) \times (V_{H_2O} + V_{Ca,added}) / 1000}{m_{sample} / (1 + 0.95)} \quad (4)$$

306 where $V_{Ca,added} = V_{Cl,added}$, $M_{Ca} = 40.08$ g/mol. It should be noted that the Ca^{2+} ions dissolved
 307 from hydration products in the pore solution are not taken into account in $C_{Ca,initial}$, but may
 308 not be excluded for $C_{Ca,eq}$.

310 **3 Results and discussion**

311 **3.1 Phase assemblages**

312 **3.1.1 Thermodynamic modeling**

313 Thermodynamic modeling is employed to predict the phase assemblages for the P, ML and M
 314 pastes exposed to the NaCl and $CaCl_2$ solutions as shown in Fig. 1. It is predicted that the main
 315 hydrates in the P paste before chloride exposure are C-S-H (Ca/Si=1.63), portlandite
 316 ($Ca(OH)_2$), ettringite ($Ca_6Al_2(SO_4)_3(OH)_{12} \cdot 26H_2O$), monocarbonate ($Ca_4Al_2CO_3(OH)_{12} \cdot 5H_2O$),
 317 calcium carbonate ($CaCO_3$) and a minor amount of hydrotalcite ($Mg_4Al_2(OH)_{14} \cdot 3H_2O$). Similar
 318 hydrates are predicted for the ML and M pastes, although the C-S-H phase exhibits a lower

351 **3.1.2 Thermogravimetric analysis**

352 The presence of Friedel's salt in the P, ML and M pastes after exposure to the NaCl and CaCl₂
353 solutions is analyzed by TGA, and the differential thermogravimetric (DTG) curves are shown
354 in Fig. 2. The DTG curves for the P paste exposed to distilled water show the presence of C-S-
355 H, ettringite and monocarbonate (50 – 300 °C), portlandite (400 – 600 °C) and calcium
356 carbonate (600 – 800 °C). For the ML and M pastes exposed to distilled water, minor amounts
357 of portlandite are still detected as a result of the heterogeneity of the hydrating material.
358 Furthermore, decomposition of strätlingite at about 250 °C is observed for the M paste. The
359 results are generally in good agreement with those observed for mortars made from the same
360 binder materials [7, 24, 26] and with the phase assemblages predicted by thermodynamic
361 modeling in Fig. 1.

362 For all pastes exposed to the NaCl and CaCl₂ solutions at high chloride concentration,
363 additional weight losses (150 – 200 °C and 280 – 400 °C) related to Friedel's salt are observed,
364 as shown in Fig. 2. The results show that the intensity of the DTG peaks associated with the six
365 main layer water molecules in Friedel's salt (280 – 400 °C) increases with increasing chloride
366 concentration. The formation of Friedel's salt at higher concentrations is accompanied by a
367 consumption of the monocarbonate and/or strätlingite phases as observed from the weight loss
368 at lower temperature around 200 – 250 °C in the DTG curves. Clearly, more Friedel's salt is
369 observed in the metakaolin containing blends, in particular in the presence of high CaCl₂
370 concentrations. The identification and transformation of phases observed by TGA confirm the
371 results predicted by thermodynamic modeling (Fig. 1).

372

373 **3.1.3 X-ray diffraction analysis**

374 The changes in phase assemblages for the P, ML and M pastes exposed to different chloride
375 concentrations of the CaCl₂ solution are also analyzed by XRD as shown in Fig. 3. The XRD
376 patterns show that the main crystalline hydration products detected in the P paste are ettringite
377 and portlandite. For the ML and M pastes, minor amounts of portlandite are detected, whereas
378 large amounts of monocarbonate and strätlingite are observed in the ML and M pastes,
379 respectively. With increasing chloride concentration from 0.25 mol/L to 1.0 mol/L and 2.0
380 mol/L, the intensity of the reflections associated with Friedel's salt increases followed by the
381 decrease of the reflection intensity for monocarbonate and strätlingite. A minor reflection
382 associated with Kuzel's salt is also detected for the M paste exposed 0.25 mol/L CaCl₂ solution.
383 The results observed from the XRD patterns confirm those observed from the DTG curves (Fig.
384 2) and those predicted by thermodynamic modeling (Fig. 1).

386 **3.2 Total chloride binding isotherms**

387 **3.2.1 Effect of the types of cations and binder composition**

388 The total chloride binding isotherms for the P, ML and M pastes exposed to the NaCl and
389 CaCl₂ solutions of varying chloride concentrations are given in Fig. 4. The isotherms are
390 calculated following the methods described in [section 2.4.4](#) by using the measured
391 concentrations presented in [Table 4](#). A higher total chloride binding is observed not only for
392 the P paste but also for the ML and M pastes when they are exposed to the CaCl₂ solution as
393 compared to the corresponding paste exposed to the NaCl solution. Similar observations for
394 chloride-exposed hydrated Portland cement can also be found in several other studies [[17](#), [32](#),
395 [35-37](#)]. This observation implies that calcium in the exposure solution plays an important role
396 in enhancing chloride binding for both hydrated Portland cement and blended cements. The
397 role of calcium on chloride binding will be further discussed in [section 3.5](#).

398 The results in [Fig. 4](#) also show that partial substitution of the wPc with MK or MK and LS
399 increases the total chloride binding. This observation is consistent with earlier studies [[13](#), [59](#)]
400 and with the higher amount of Friedel's salt in the blended cement systems predicted by
401 thermodynamic modeling ([Fig. 1](#)). There is no major difference in total chloride binding
402 between the ML and M pastes.

403

404 **3.3 Assessment of the chloride distribution in solids**

405 **3.3.1 Chloride bound as Friedel's salt**

406 The present work utilizes the results of the degree of reaction for the principal phases from a
407 ²⁹Si NMR study of paste samples of the same blends by Dai [[43](#)] in combination with
408 thermodynamic modeling to quantify the amount of Friedel's salt formed. The results are
409 compared with those from XRD/Rietveld analysis performed on several selected samples as
410 shown in [Fig. 5a](#). The good agreement between the thermodynamic calculations and
411 XRD/Rietveld analysis suggests a reliable prediction of the Friedel's salt content from
412 thermodynamic modeling. The calculated amounts of Cl bound as Friedel's salt by
413 thermodynamic modeling is presented in [Fig. 5b](#). For the P pastes, the results show that the
414 constant (maximum) amount of chloride binding by the formation of Friedel's salt is
415 independent on the type of cations. Based on the obtained amount of Friedel's salt together
416 with the calcium aluminate (C₃A) content of the studied Portland cement, it can be calculated
417 that only 20 % of the C₃A is consumed for the formation of the actual amounts of Friedel's salt,

418 which is consistent with the fraction determined for chloride exposed mortars in a parallel
419 study [7]. The main fraction of aluminum remains in the ettringite phase as predicted by
420 thermodynamic modeling. For the ML and M pastes, thermodynamic modeling shows that the
421 maximum binding capacity with respect to transformation of the maximum amount of
422 monocarbonate has not been obtained for the ML and M pastes exposed to the NaCl solution
423 (Fig. 1c,e). This is related to the limited availability of calcium, which prevents the further
424 formation of Friedel's salt as exemplified in Eq. (7). Similar to the present study, an earlier
425 study of ten hydrated cement pastes containing limestone and different pozzolanic materials
426 [60] reported that the presence of alkalis hinders the formation of chloride-bearing AFm phases.
427 According to the present work, this can be explained by an insufficient amount of calcium in
428 the exposure solution, inhibiting the transformation of strätlingite and/or monocarbonate to
429 Friedel's salt according to Eqs. (5), (6) and (7). For all samples, thermodynamic modeling also
430 predicts that the formation of Friedel's salt starts at lower chloride concentration for the CaCl₂
431 exposure as compared to the NaCl exposure, (e.g. 0.2 mol/L vs. 0.4 mol/L for ML pastes). This
432 finding indicates that calcium plays an important role in facilitating the formation of Friedel's
433 salt.

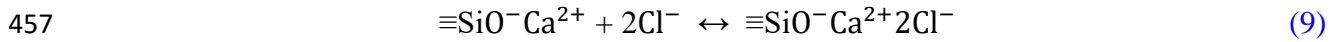
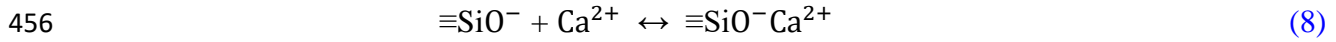
434 Several studies have reported that the addition of alumina-rich SCMs increase the chloride
435 binding due to formation of an additional amount of Friedel's salt. This is confirmed in the
436 present study by thermodynamic modeling and the amounts of Friedel's salt obtained from
437 XRD/Rietveld analysis in Fig. 5. Both the experimental and thermodynamic modeling data
438 show that a higher amount of Friedel's salt is formed for the metakaolin blends as compared to
439 the plain Portland cement.

440

441 3.3.2 Chloride associated with C-S-H

442 An attempt to evaluate the relative differences in chloride content associated with the C-S-H
443 phase is made for the samples exposed to chloride solutions with different associated cations
444 (*i.e.*, Na⁺ and Ca²⁺). No significant chloride binding in the C-S-H phase is observed for the M
445 and ML pastes as seen by comparing the data from Fig. 4b and Fig. 5b. The chloride ions
446 associated with the C-S-H in the P samples are shown in Fig. 6. These data are obtained by
447 subtracting the chloride bound as Friedel's salt obtained from thermodynamic modelling from
448 the amount of total bound chloride. For the P sample (Fig.6a), it is clear that the presence of an
449 additional amount of Ca²⁺ ions in the exposure solution increases the amount of chloride in the
450 diffuse layer of the C-S-H phase as compared to the NaCl solution. According to the studies of
451 Nonat and coworkers [28, 61], this can be explained by the sorption of calcium onto the

452 negatively charged C-S-H surface, according to Eq. (8), which can lead to a positively charged
 453 surface at higher calcium concentrations. In the presence of chloride, this positively charged
 454 surface is compensated by chloride ions in the diffuse layer of the C-S-H phase according to Eq.
 455 (9) as described in earlier studies [28, 30].



458

459 **3.3.3 Contribution from Friedel's salt and the C-S-H phase to the total chloride binding**

460 Based on the discussion above, the contribution from Friedel's salt and the C-S-H phase to the
 461 total chloride binding can potentially be evaluated. For the P paste exposed to the NaCl
 462 solution, the total chloride binding and its maximum binding capacity (Fig. 4a) are mainly
 463 determined by the chloride binding as Friedel's salt. When the P paste is exposed to the CaCl₂
 464 solution, the higher and continuous increase in the total chloride binding (Fig. 4b) originates
 465 from chloride in the diffuse layer of the C-S-H (Fig. 6a), since the maximum chloride binding
 466 as Friedel's salt is reached (Fig. 5b). An increase in the total chloride binding is observed when
 467 metakaolin is used to replace Portland cement (Fig. 4a, b), which is ascribed to the formation
 468 of more Friedel's salt rather than chloride binding in the C-S-H phase, since there is no clear
 469 evidence of a chloride adsorption on the C-S-H phase in the ML and M pastes.

470

471 **3.4 pH values**

472 **3.4.1 Effect of the exposure solution on pH**

473 The measured pH values for the supernatants of the NaCl and CaCl₂ exposure solutions for the
 474 P, ML and M pastes are shown in Table 4 and Fig. 7. The results show a lower pH for the ML
 475 and M pastes than for the P paste as already observed for hydrated blended cements [62]. There
 476 is a minor increase in pH when the pastes are exposed to NaCl solutions compared to the pastes
 477 exposed to distilled water, which has also been observed earlier [37]. The increased pH in the
 478 presence of NaCl(aq) is assumed to be related to the conversion of monocarbonate and
 479 portlandite to Friedel's salt, calcium carbonate and sodium hydroxide as described by Eq. (5),
 480 which results in an increase of the OH⁻(aq) concentration. A significant decrease in pH is
 481 observed with increasing chloride concentrations when the pastes are exposed to the CaCl₂
 482 solutions as also reported in other studies [36, 37, 63]. The decrease in pH upon the presence of
 483 CaCl₂(aq) is not related to the conversion of monocarbonate to Friedel's salt (see Eq. (6)), but
 484 it may be caused by a calcium uptake by the C-S-H phase, since at high calcium concentrations,

485 Ca^{2+} can be adsorbed on the surface of the C-S-H [30, 61, 64], leading to a release of charge
486 balancing H^+ ions from the silanol groups to the exposure solution according to Eq. (8).

487

488 **3.4.2 Relationship between pH and chloride binding**

489 The relationship between the total amount of bound chloride and the pH of the exposure
490 solutions for P, ML and M pastes exposed to the NaCl and CaCl_2 solutions are shown in Fig. 8.
491 Since the changes in pH for the NaCl exposure solutions are small, only a minor effect of pH
492 on the binding is observed and the increased chloride binding for the pastes exposed to NaCl
493 solutions is mainly driven by the formation of Friedel's salt. In contrast, an apparent
494 correlation between the total bound chloride and pH is obtained for the P paste exposed to the
495 CaCl_2 solution (Fig. 8a) as reported recently [37]. For the P paste, a small fraction of chloride
496 can be bound in Friedel's salt as the studied Portland cement only forms a small amount of
497 AFm phases upon hydration. The additional uptake observed in the presence of $\text{CaCl}_2(aq)$ but
498 not in the case of $\text{NaCl}(aq)$ is thus related to chloride ions present in the diffuse layer of C-S-H.
499 A similar increase of chloride binding with decreasing pH has also been reported in earlier
500 studies [36, 37, 63]. The increased total chloride binding with lower pH has been ascribed to
501 less competition with OH^- ions and thus a larger Cl^- uptake by the C-S-H [36, 38]. A similar
502 correlation can also be observed for the blended cements containing metakaolin with or
503 without limestone exposed to the CaCl_2 solution (Fig. 8b). Different from the P paste, the
504 additional uptake of chloride observed for the M and ML pastes in the presence of the CaCl_2
505 solution compared to the NaCl solution is related to chloride ions present in Friedel's salt and
506 not in the diffuse layer of the C-S-H (Fig. 5b).

507

508 **3.5 Role of calcium in chloride binding**

509 **3.5.1 Relationship between pH and the calcium concentration**

510 The impact of cations on chloride binding is related to the availability of calcium as discussed
511 above for Friedel's salt and as observed by the amount of chloride ions in the diffuse layer of
512 the C-S-H in published studies [28, 30]. The apparent pH dependency of the chloride binding
513 in the case of CaCl_2 exposure (Fig. 8) can be explained by the intrinsic relation between pH
514 and the calcium concentrations of the pore solution as shown in Fig. 9, which is constructed
515 using the data in Table 4. The results show that the pH decreases with increased CaCl_2
516 concentration for the exposure solution for all the studied cement pastes. For this reason, the
517 uptake of calcium from the CaCl_2 exposure solution and its effect on the amount of total bound
518 chloride and chloride associated with the C-S-H will be evaluated in more detail below.

519
520 **3.5.2 Total calcium binding from the CaCl₂ solution**
521 Similar to chloride binding, also the calcium ions added are taken up by cement hydrates in the
522 P, ML and M pastes as shown in Fig. 10. The uptake of calcium by the cement pastes increases
523 with increasing CaCl₂ concentration in the exposure solution, as expected. This trend is found
524 to be similar to that of the total chloride binding isotherm (Fig. 4). The increment of both the
525 calcium and chloride binding decreases at high chloride concentration, indicating that a
526 maximum calcium and chloride binding capacity is present in the hydrated cement blends. In
527 addition, both the calcium and chloride binding are found to be higher for the ML and M pastes
528 than for the P paste as expected, since a larger amount of calcium ions are needed to
529 accommodate the released carbonate from monocarbonate for the formation of Friedel's salt.

530
531 **3.5.3 Relationship between bound chloride and bound calcium**

532 The relationship between total bound chloride and total "bound" calcium (*i.e.*, uptake of
533 calcium from the CaCl₂ exposure solution by hydration products) for the studied pastes is
534 shown in Fig. 11. The data show a linear correlation between the amount of total bound
535 chloride and the total "bound" calcium content from the CaCl₂ solution. More interestingly, the
536 ratio between total bound chloride and calcium is close to Cl/Ca = 2, independent of the type of
537 studied cement blend. The linear correlation between the bound Ca and bound chloride is
538 ascribed to the following mechanisms: (i) calcium promotes the formation of Friedel's salt
539 (uptake of two chloride ions) plus CaCO₃ (one calcium) from monocarbonate according to Eq.
540 (6) and (ii) calcium increases the amount of chloride in the diffuse layer of the C-S-H, as
541 shown by Eq. (9) and discussed in a recent study [30]. Overall, the results confirm that the
542 amount of bound calcium has a closer relation with the chloride binding than effects from pH.
543 No relationship between the bound chloride and bound calcium can be obtained for the P, ML
544 and M pastes exposed to the NaCl solutions, which reflects that no additional calcium is
545 introduced into these systems.

546
547 **4 Conclusions**

548 The chloride binding of Portland cement (P) – metakaolin (M) – limestone (L) blends exposed
549 to different concentrations of NaCl and CaCl₂ solutions has been investigated and based on the
550 analysis of the results from TGA, XRD, exposure solution elemental analysis and
551 thermodynamic modeling, the following conclusions can be drawn:

552 (1) The use of metakaolin in Portland cement blends increases the chloride-binding capacity
553 compared to pure Portland cement. This is attributed to the formation of a larger quantity of
554 Friedel's salt in the ML and M samples as compared to the P samples and it reflects that
555 metakaolin acts as an additional aluminum source.

556 (2) A larger quantity of chloride is bound in the P samples exposed to the CaCl_2 solution as
557 compared to the NaCl solution. This is ascribed to the higher amount of available calcium ions,
558 which enhances the presence of chloride ions in the diffuse layer of the C-S-H, whereas the
559 amount of Friedel's salt is independent of the type of cation in the NaCl or CaCl_2 exposure
560 solutions. For the ML and M samples exposed to the CaCl_2 solution, the increased chloride
561 binding, as compared to NaCl exposure solution, is ascribed to the higher calcium
562 concentrations, which increase the formation of Friedel's salt. A schematic drawing
563 summarizing the distribution of chloride ions in the hydrated cement blends is shown in [Fig. 12](#).

564 (3) The pH is found to decrease with increasing CaCl_2 concentration as a result of the calcium
565 binding on the C-S-H surface resulting in a release of protons, whereas a minor increase in pH
566 is observed for increasing NaCl concentration as a result of the conversion of monocarbonate
567 to Friedel's salt and calcium carbonate.

568 (4) Independent of the type of cement blends, the present results indicate that the calcium
569 concentration has a decisive role for the chloride binding as the uptake of chloride is found to
570 be coupled with the consumption of calcium from the exposure solution. A linear correlation
571 between the amounts of total bound chloride and total "bound" calcium from the CaCl_2
572 exposure solution has been established with a Cl/Ca ratio close to 2:1.

573

574 **Acknowledgements**

575 The Danish Council for Strategic Research is acknowledged for financial support to the LowE-
576 CEM project (No. 11-116724).

577

578 **References**

- 579 [1] L. Bertolini, B. Elsener, P. Pedferri, E. Redaelli, R.B. Polder, Corrosion of steel in
580 concrete: prevention, diagnosis, repair, John Wiley & Sons, 2013.
- 581 [2] Q. Yuan, C. Shi, G. De Schutter, K. Audenaert, D. Deng, Chloride binding of cement-
582 based materials subjected to external chloride environment—a review, *Construction and*
583 *Building Materials*, 23 (2009) 1-13.
- 584 [3] U. Angst, B. Elsener, C.K. Larsen, Ø. Vennesland, Critical chloride content in reinforced
585 concrete—a review, *Cement and Concrete Research*, 39 (2009) 1122-1138.
- 586 [4] X. Shi, N. Xie, K. Fortune, J. Gong, Durability of steel reinforced concrete in chloride
587 environments: An overview, *Construction and Building Materials*, 30 (2012) 125-138.
- 588 [5] I. Galan, F.P. Glasser, Chloride in cement, *Advances in Cement Research*, 27 (2015) 63-
589 97.
- 590 [6] R. Loser, B. Lothenbach, A. Leemann, M. Tuchschnid, Chloride resistance of concrete
591 and its binding capacity—Comparison between experimental results and thermodynamic
592 modeling, *Cement and Concrete Composites*, 32 (2010) 34-42.
- 593 [7] Z. Shi, M.R. Geiker, B. Lothenbach, K. De Weerd, S. Ferreira Garzón, K. Enemark-
594 Rasmussen, J. Skibsted, Friedel's salt profiles from thermogravimetric analysis and
595 thermodynamic modelling of Portland cement-based mortars exposed to sodium
596 chloride solution, *Cement and Concrete Composites*, (in press 2017).
- 597 [8] V. Baroghel-Bouny, X. Wang, M. Thiery, M. Saillio, F. Barberon, Prediction of chloride
598 binding isotherms of cementitious materials by analytical model or numerical inverse
599 analysis, *Cement and Concrete Research*, 42 (2012) 1207-1224.
- 600 [9] D.P. Bentz, E.J. Garboczi, Y. Lu, N. Martys, A.R. Sakulich, W.J. Weiss, Modeling of the
601 influence of transverse cracking on chloride penetration into concrete, *Cement and*
602 *Concrete Composites*, 38 (2013) 65-74.
- 603 [10] G.K. Glass, N.R. Buenfeld, The influence of chloride binding on the chloride induced
604 corrosion risk in reinforced concrete, *Corrosion Science*, 42 (2000) 329-344.
- 605 [11] B. Martín-Pérez, H. Zibara, R. Hooton, M. Thomas, A study of the effect of chloride
606 binding on service life predictions, *Cement and Concrete Research*, 30 (2000) 1215-
607 1223.
- 608 [12] E. L'Hôpital, N. Seigneur, M. Voutilainen, A. Dauzères, Transport properties of cement
609 model system (C3S and C-S-H): Experiments dedicated to implement a new approach
610 of the microstructure / diffusion properties relation in the reactive transport code, in:

- 611 4th International Workshop on Mechanisms and Modelling of Waste / Cement
612 Interactions May 22-25, 2016, Murten, Switzerland, 2016.
- 613 [13] M. Thomas, R. Hooton, A. Scott, H. Zibara, The effect of supplementary cementitious
614 materials on chloride binding in hardened cement paste, *Cement and Concrete*
615 *Research*, 42 (2012) 1-7.
- 616 [14] R. Dhir, M. El-Mohr, T. Dyer, Chloride binding in GGBS concrete, *Cement and Concrete*
617 *Research*, 26 (1996) 1767-1773.
- 618 [15] R. Luo, Y. Cai, C. Wang, X. Huang, Study of chloride binding and diffusion in GGBS
619 concrete, *Cement and Concrete Research*, 33 (2003) 1-7.
- 620 [16] R.K. Dhir, M.A.K. El-Mohr, T.D. Dyer, Developing chloride resisting concrete using
621 PFA, *Cement and Concrete Research*, 27 (1997) 1633-1639.
- 622 [17] C. Arya, N. Buenfeld, J. Newman, Factors influencing chloride-binding in concrete,
623 *Cement and Concrete Research*, 20 (1990) 291-300.
- 624 [18] C. Arya, Y. Xu, Effect of cement type on chloride binding and corrosion of steel in
625 concrete, *Cement and Concrete Research*, 25 (1995) 893-902.
- 626 [19] C.S. Poon, S.C. Kou, L. Lam, Compressive strength, chloride diffusivity and pore
627 structure of high performance metakaolin and silica fume concrete, *Construction and*
628 *Building Materials*, 20 (2006) 858-865.
- 629 [20] S. Wild, J. Khatib, A. Jones, Relative strength, pozzolanic activity and cement hydration
630 in superplasticised metakaolin concrete, *Cement and Concrete Research*, 26 (1996)
631 1537-1544.
- 632 [21] K. De Weerd, K. Kjellsen, E. Sellevold, H. Justnes, Synergy between fly ash and
633 limestone powder in ternary cements, *Cement and Concrete Composites*, 33 (2011) 30-
634 38.
- 635 [22] K. De Weerd, H. Justnes, K.O. Kjellsen, E. Sellevold, Fly ash-limestone ternary
636 composite cements: synergetic effect at 28 days, *Nordic Concrete Research*, 42 (2010)
637 51-70.
- 638 [23] M. Steenberg, D. Herfort, S. Poulsen, J. Skibsted, J. Damtoft, Composite cement based on
639 Portland cement clinker, limestone and calcined clay, in: *13th International Congress*
640 *of the Chemistry of Cement*, Madrid, 2011, pp. 97.
- 641 [24] M. Antoni, J. Rossen, F. Martirena, K. Scrivener, Cement substitution by a combination
642 of metakaolin and limestone, *Cement and Concrete Research*, 42 (2012) 1579-1589.

- 643 [25] K. Scrivener, A. Favier, (Eds.). *Calcined Clays for Sustainable Concrete: Proceedings of*
644 *the 1st International Conference on Calcined Clays for Sustainable Concrete*, Springer,
645 2015.
- 646 [26] Z. Shi, B. Lothenbach, M.R. Geiker, J. Kaufmann, A. Leemann, S. Ferreiro, J. Skibsted,
647 *Experimental studies and thermodynamic modeling of the carbonation of Portland*
648 *cement, metakaolin and limestone mortars*, *Cement and Concrete Research*, 88 (2016)
649 60-72.
- 650 [27] Z. Shi, M.R. Geiker, K. De Weerd, B. Lothenbach, J. Kaufmann, W. Kunther, S.
651 *Ferreiro, D. Herfort, J. Skibsted, Durability of Portland cement blends including*
652 *calcined clay and limestone: interactions with sulfate, chloride and carbonate ions*, in:
653 *Calcined Clays for Sustainable Concrete*, Springer, 2015, pp. 133-141.
- 654 [28] G. Plusquellec, A. Nonat, *Interactions between calcium silicate hydrate (C-S-H) and*
655 *calcium chloride, bromide and nitrate*, *Cement and Concrete Research*, 90 (2016) 89-
656 96.
- 657 [29] J.J. Beaudoin, V.S. Ramachandran, R.F. Feldman, *Interaction of chloride and CSH*,
658 *Cement and Concrete Research*, 20 (1990) 875-883.
- 659 [30] G. Plusquellec, A. Nonat, I. Pochard, *Anion uptake by calcium silicate hydrate. 32nd*
660 *Cement and Concrete Science Conference. Belfast. 17 - 18 Sept. 2012 (paper PRE-4)*,
661 (2012).
- 662 [31] V.S. Ramachandran, *Possible states of chloride in the hydration of tricalcium silicate in*
663 *the presence of calcium chloride*, *Matériaux et Construction*, 4 (1971) 3-12.
- 664 [32] O. Wowra, M.J. Setzer, *Sorption of chlorides on hydrated cement and C3S pastes*, in:
665 *M.J. Setzer, R. Auberg (Eds.) "Frost Resistance of Concrete" Proceedings of the*
666 *International RILEM Workshop on Resistance of Concrete to Freezing and Thawing*
667 *With or Without De-icing Chemicals E & FN Spon, London SE1 8HN, UK, 1997, pp.*
668 *155-162.*
- 669 [33] L. Tang, L.-O. Nilsson, *Chloride binding capacity and binding isotherms of OPC pastes*
670 *and mortars*, *Cement and Concrete Research*, 23 (1993) 247-253.
- 671 [34] H. Zibara, R. Hooton, M. Thomas, K. Stanish, *Influence of the C/S and C/A ratios of*
672 *hydration products on the chloride ion binding capacity of lime-SF and lime-MK*
673 *mixtures*, *Cement and Concrete Research*, 38 (2008) 422-426.
- 674 [35] A. Delagrave, J. Marchand, J.-P. Ollivier, S. Julien, K. Hazrati, *Chloride binding capacity*
675 *of various hydrated cement paste systems*, *Advanced Cement Based Materials*, 6 (1997)
676 28-35.

- 677 [36] J. Tritthart, Chloride binding in cement II. The influence of the hydroxide concentration
678 in the pore solution of hardened cement paste on chloride binding, *Cement and*
679 *Concrete Research*, 19 (1989) 683-691.
- 680 [37] K. De Weerd, A. Colombo, L. Coppola, H. Justnes, M. Geiker, Impact of the associated
681 cation on chloride binding of Portland cement paste, *Cement and Concrete Research*,
682 68 (2015) 196-202.
- 683 [38] A. Suryavanshi, J. Scantlebury, S. Lyon, Mechanism of Friedel's salt formation in
684 cements rich in tri-calcium aluminate, *Cement and Concrete Research*, 26 (1996) 717-
685 727.
- 686 [39] F. Pruckner, O. Gjrv, Effect of CaCl₂ and NaCl additions on concrete corrosivity,
687 *Cement and Concrete Research*, 34 (2004) 1209-1217.
- 688 [40] Q. Zhu, L. Jiang, Y. Chen, J. Xu, L. Mo, Effect of chloride salt type on chloride binding
689 behavior of concrete, *Construction and Building Materials*, 37 (2012) 512-517.
- 690 [41] K. De Weerd, D. Orskov, M. Geiker, The impact of sulphate and magnesium on
691 chloride binding in Portland cement paste, *Cement and Concrete Research*, 65 (2014)
692 30-40.
- 693 [42] S.L. Poulsen, V. Kocaba, G. Le Saot, H.J. Jakobsen, K.L. Scrivener, J. Skibsted,
694 Improved quantification of alite and belite in anhydrous Portland cements by ²⁹Si
695 MAS NMR: Effects of paramagnetic ions, *Solid State Nuclear Magnetic Resonance*, 36
696 (2009) 32-44.
- 697 [43] Z. Dai, Solid-state ²⁷Al and ²⁹Si MAS NMR investigations of white Portland cement -
698 metakaolin blends (PhD thesis), Aarhus University, in, 2015.
- 699 [44] K.O. Kjellsen, R.J. Detwiler, O.E. Gjrv, Development of microstructures in plain
700 cement pastes hydrated at different temperatures, *Cement and Concrete Research*, 21
701 (1991) 179-189.
- 702 [45] T. Wagner, D.A. Kulik, F.F. Hingerl, S.V. Dmytrieva, GEM-Selektor geochemical
703 modeling package: TSolMod library and data interface for multicomponent phase
704 models, *The Canadian Mineralogist*, 50 (2012) 1173-1195.
- 705 [46] D.A. Kulik, T. Wagner, S.V. Dmytrieva, G. Kosakowski, F.F. Hingerl, K.V. Chudnenko,
706 U.R. Berner, GEM-Selektor geochemical modeling package: revised algorithm and
707 GEMS3K numerical kernel for coupled simulation codes, *Computational Geosciences*,
708 17 (2013) 1-24.
- 709 [47] D.A. Kulik, Improving the structural consistency of CSH solid solution thermodynamic
710 models, *Cement and Concrete Research*, 41 (2011) 477-495.

- 711 [48] H.C. Helgeson, D.H. Kirkham, G.C. Flowers, Theoretical prediction of the
712 thermodynamic behavior of aqueous electrolytes by high pressures and temperatures;
713 IV, Calculation of activity coefficients, osmotic coefficients, and apparent molal and
714 standard and relative partial molal properties to 600 degrees C and 5kb, American
715 Journal of Science, 281 (1981) 1249-1516.
- 716 [49] B.J. Merkel, B. Planer-Friedrich, D. Nordstrom, Groundwater geochemistry, Springer-
717 Verlag Berlin Heidelberg, 2005.
- 718 [50] B. Lothenbach, G. Le Saout, M.B. Haha, R. Figi, E. Wieland, Hydration of a low-alkali
719 CEM III/B–SiO₂ cement (LAC), Cement and Concrete Research, 42 (2012) 410-423.
- 720 [51] D. Kulik, J. Tits, E. Wieland, Aqueous-solid solution model of strontium uptake in CSH
721 phases, Geochimica et Cosmochimica Acta, 71 (2007) A530.
- 722 [52] R. Barbarulo, Comportement des matériaux cimentaires: actions des sulfates et de la
723 température (Ph.D. thesis), in, Université Laval Québec, 2002.
- 724 [53] M. Balonis, B. Lothenbach, G. Le Saout, F.P. Glasser, Impact of chloride on the
725 mineralogy of hydrated Portland cement systems, Cement and Concrete Research, 40
726 (2010) 1009-1022.
- 727 [54] U. Birnin-Yauri, F. Glasser, Friedel's salt, Ca₂Al(OH)₆(Cl,OH)·2H₂O: its solid solutions
728 and their role in chloride binding, Cement and Concrete Research, 28 (1998) 1713-
729 1723.
- 730 [55] R.O. Grishchenko, A.L. Emelina, P.Y. Makarov, Thermodynamic properties and thermal
731 behavior of Friedel's salt, Thermochemica Acta, 570 (2013) 74-79.
- 732 [56] B. Lothenbach, P. Durdziński, K. De Weerd, Thermogravimetric analysis, in: K.
733 Scrivener, R. Snellings, B. Lothenbach (Eds.) A Practical Guide to Microstructural
734 Analysis of Cementitious Materials, CRC Press, 2016, pp. 177.
- 735 [57] R. Snellings, X-ray powder diffraction applied to cement, in: K. Scrivener, R. Snellings,
736 B. Lothenbach (Eds.) A Practical Guide to Microstructural Analysis of Cementitious
737 Materials, CRC Press, 2016, pp. 107-176.
- 738 [58] Y. Elakneswaran, T. Nawa, K. Kurumisawa, Electrokinetic potential of hydrated cement
739 in relation to adsorption of chlorides, Cement and Concrete Research, 39 (2009) 340-
740 344.
- 741 [59] N.J. Coleman, C.L. Page, Aspects of the pore solution chemistry of hydrated cement
742 pastes containing metakaolin, Cement and Concrete Research, 27 (1997) 147-154.

- 743 [60] A. Ipavec, T. Vuk, R. Gabrovšek, V. Kaučič, Chloride binding into hydrated blended
744 cements: The influence of limestone and alkalinity, *Cement and Concrete Research*, 48
745 (2013) 74-85.
- 746 [61] C. Labbez, I. Pochard, B. Jönsson, A. Nonat, CSH/solution interface: Experimental and
747 Monte Carlo studies, *Cement and Concrete Research*, 41 (2011) 161-168.
- 748 [62] B. Lothenbach, K. Scrivener, R.D. Hooton, Supplementary cementitious materials,
749 *Cement and Concrete Research*, 41 (2011) 1244-1256.
- 750 [63] H. Zibara, Binding of external chlorides by cement pastes. (PhD thesis), University of
751 Toronto, Canada., (2001).
- 752 [64] B. Lothenbach, A. Nonat, Calcium silicate hydrates: Solid and liquid phase composition,
753 *Cement and Concrete Research*, 78 (2015) 57-70.
754
755

756 **Table 1**

757 Chemical compositions (wt.%), density and Blaine fineness for the starting materials.

	wPc	LS	MK
SiO ₂	21.81	3.92	52.84
Al ₂ O ₃	3.56	0.33	39.49
Fe ₂ O ₃	0.24	0.14	1.42
CaO	66.13	53.73	0.22
MgO	1.10	0.35	0.48
K ₂ O	0.43	0.05	1.00
Na ₂ O	0.04	0.08	0.05
SO ₃	3.37	0.05	0.06
TiO ₂	0.21	0.02	0.88
P ₂ O ₅	0.04	0.10	0.11
LOI	2.57	41.8	3.55
Density (kg/m ³)	3080	2700	2530
Blaine fineness (m ² /kg)	387	1211	1891
Carbon content	0.37	-	-
CaCO ₃	3.1	93.8	-

758

759

760 **Table 2**

761 Binder compositions for the produced mortars (wt.%).

Blend	wPc ^a	MK	LS ^a	Al/Si ^b	S/Si ^c
				C-S-H (mol/mol)	
P	100	0	0	0.067	0.03
ML	68.1	25.5	6.4	0.092	0.015
M	68.1	31.9	0	0.1	0.015

762 ^(a) The wPc contains 3.1 wt.% limestone. Thus, the Portland clinker replacement level is 35.0
 763 wt% for the ML and M blends.

764 ^(b) Al/Si ratios determined from ²⁹Si MAS NMR for paste samples of the same blends [43].

765 ^(c) S/Si ratios determined for synthetic C-S-H samples with different Ca/Si ratios [52]. The data
 766 are related to the individual samples using the Ca/Si ratios determined for the C-S-H phases in
 767 the paste samples in ref. [43].

768 **Table 3**

769 Degrees of hydration (H , %)^a for alite, belite and MK in hydrated paste samples after 28 – 182
 770 days of hydration in demineralized water [43].

Blend	Alite		belite		MK	
	28d	180d	28d	180d	28d	180d
P	81	95	25	63		
ML	83	86	34	36	48	54
M	86	86	34	34	38	50

771 ^a Determined from ²⁹Si MAS NMR [43] as $H = (1 - I(t)/I(t=0))$, where $I(t=0)$ and $I(t)$ are the
 772 intensities of the individual phases before and after hydration for the time (t), respectively.

773

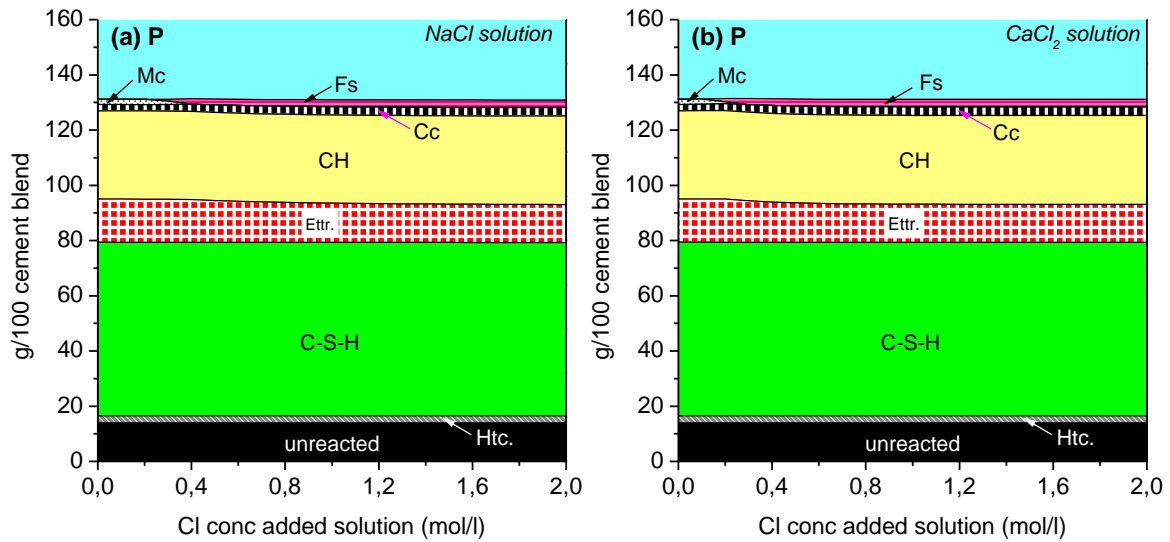
774 **Table 4**

775 Measured chloride and calcium concentrations and pH values of the exposure solutions at
 776 equilibrium.

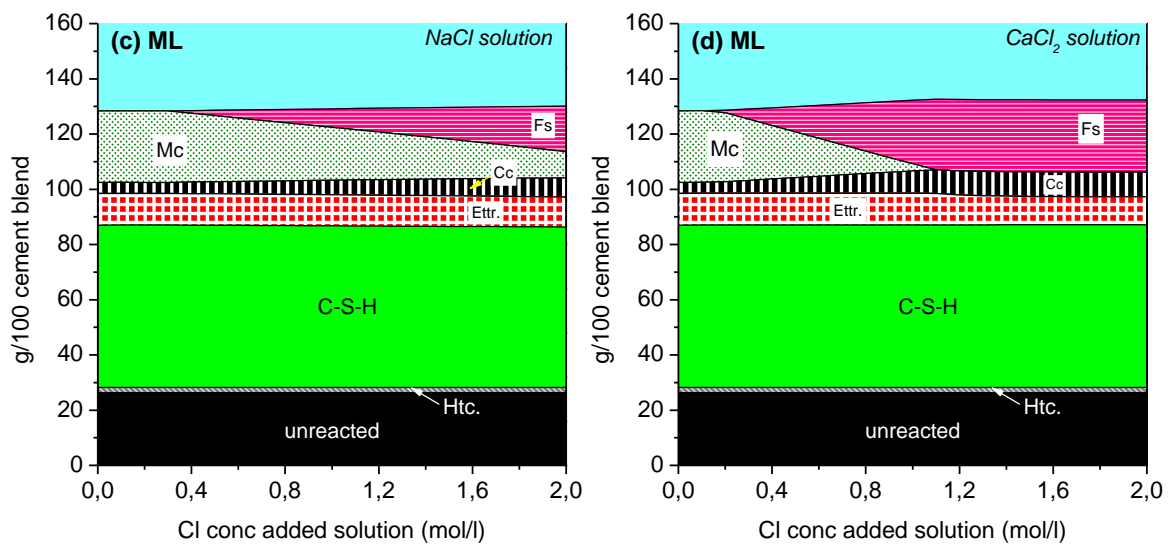
Blend	$C_{Cl,added}$ [M]	Replicates ^a	NaCl					CaCl ₂				
			$C_{Cl,eq}$ [M]	Errors [M]	$C_{Ca,eq}$ [mM]	Errors [mM]	pH	$C_{Cl,eq}$ [M]	Errors [M]	$C_{Ca,eq}$ [mM]	Errors [mM]	pH
P	0	1	0.001	-	10.2	-	12.9	-	-	-	-	12.9
	0.125	2	0.031	0.001	11.9	2.4	13.0	0.019	0.002	15.8	1.7	12.8
	0.25	2	0.081	0.001	8.2	0.34	13.1	0.047	0.000	23.5	1.7	12.8
	0.50	3	0.213	0.008	7.1	0.43	13.1	0.114	0.004	49.1	1.1	12.6
	1.0	3	0.476	0.013	7.3	0.36	13.1	0.285	0.004	126	1.7	12.4
	2.0	2	1.078	0.017	7.5	0.03	13.0	0.695	0.006	349	6.5	12.1
ML	0	1	-	-	-	-	12.4	-	-	-	-	12.4
	0.125	2	0.012	0.001	1.6	0.76	12.6	0.005	0.001	5.5	3.6	12.4
	0.25	2	0.036	0.000	1.2	0.22	12.7	0.012	0.000	3.2	0.3	12.3
	0.50	3	0.137	0.002	1.0	0.11	12.6	0.042	0.001	10.1	0.6	12.1
	1.0	3	0.359	0.002	1.6	0.25	12.6	0.123	0.003	50.4	3.8	11.8
	2.0	2	0.862	0.027	1.6	0.04	12.6	0.491	0.011	227	0.3	11.4
M	0	1	0.001	-	2.8	-	12.4	-	-	-	-	12.4
	0.125	2	0.012	0.000	1.4	0.19	12.6	0.005	0.000	4.6	-	12.3
	0.25	2	0.047	0.001	1.3	0.17	12.6	0.017	0.001	5.0	0.1	12.2
	0.50	3	0.152	0.007	1.6	0.5	12.6	0.045	0.001	10.8	1.9	12.0
	1.0	3	0.369	0.009	3.8	2.8	12.5	0.122	0.003	56.4	4.4	11.3
	2.0	2	0.892	0.001	2.0	0.14	12.4	0.419	0.013	223	-	10.8

777 ^a The measured chloride and calcium concentrations are the average of the values for the
 778 number of replicates.

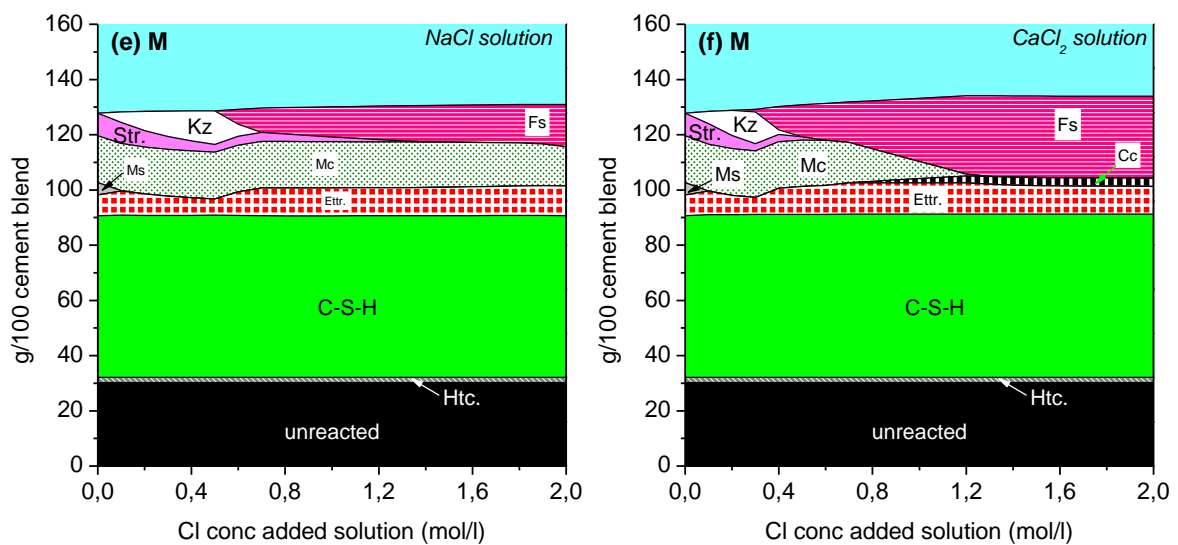
779



780



781

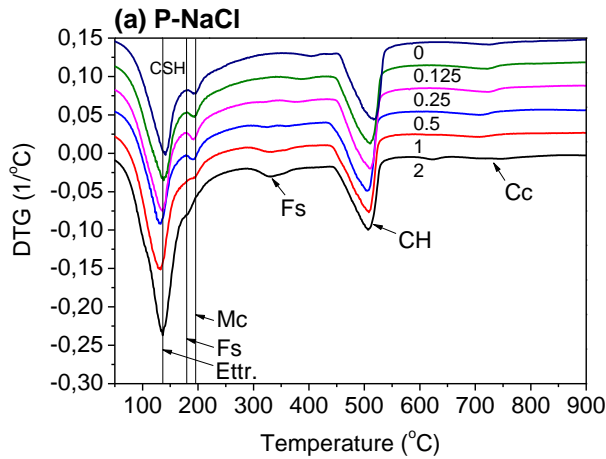


782

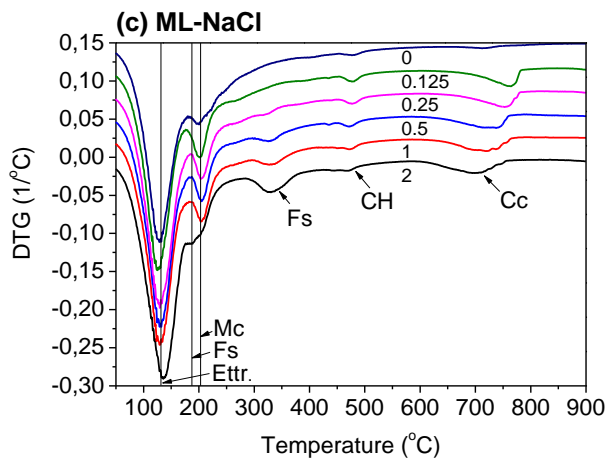
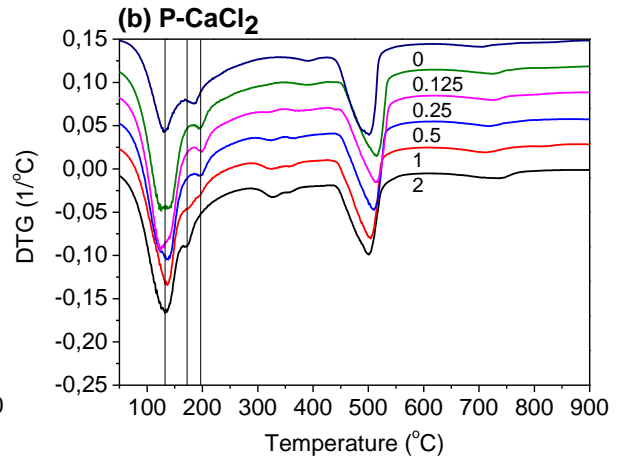
783 **Fig. 1.** Phase assemblages for the P, ML and M pastes exposed to the NaCl and CaCl₂ solutions.

784 C-S-H: calcium-silicate-hydrate; Etrr.: ettringite; CH: portlandite; Mc: monocarbonate; Str.:

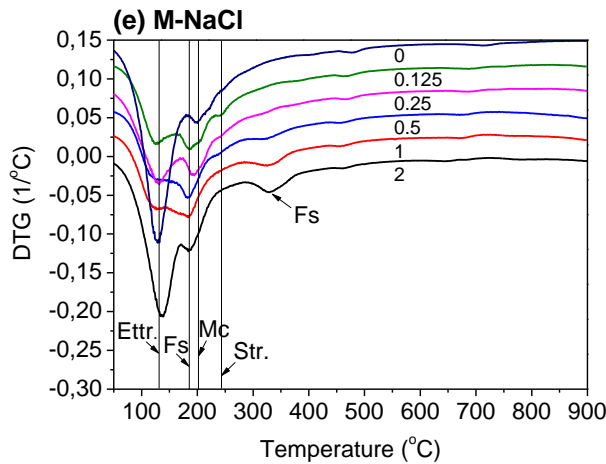
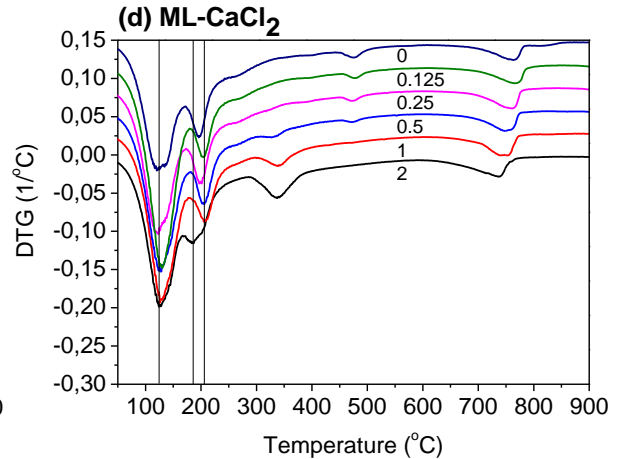
785 strätlingite; Cc: CaCO₃; Fs: Friedel's salt; Kz: Kuzel's salt; Htc.: Hydrotalcite.



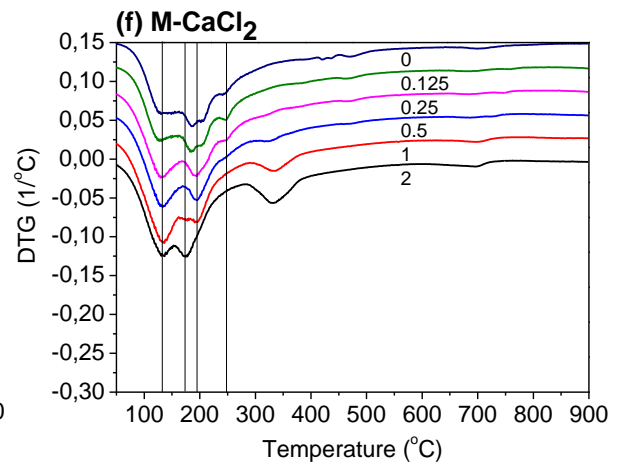
786



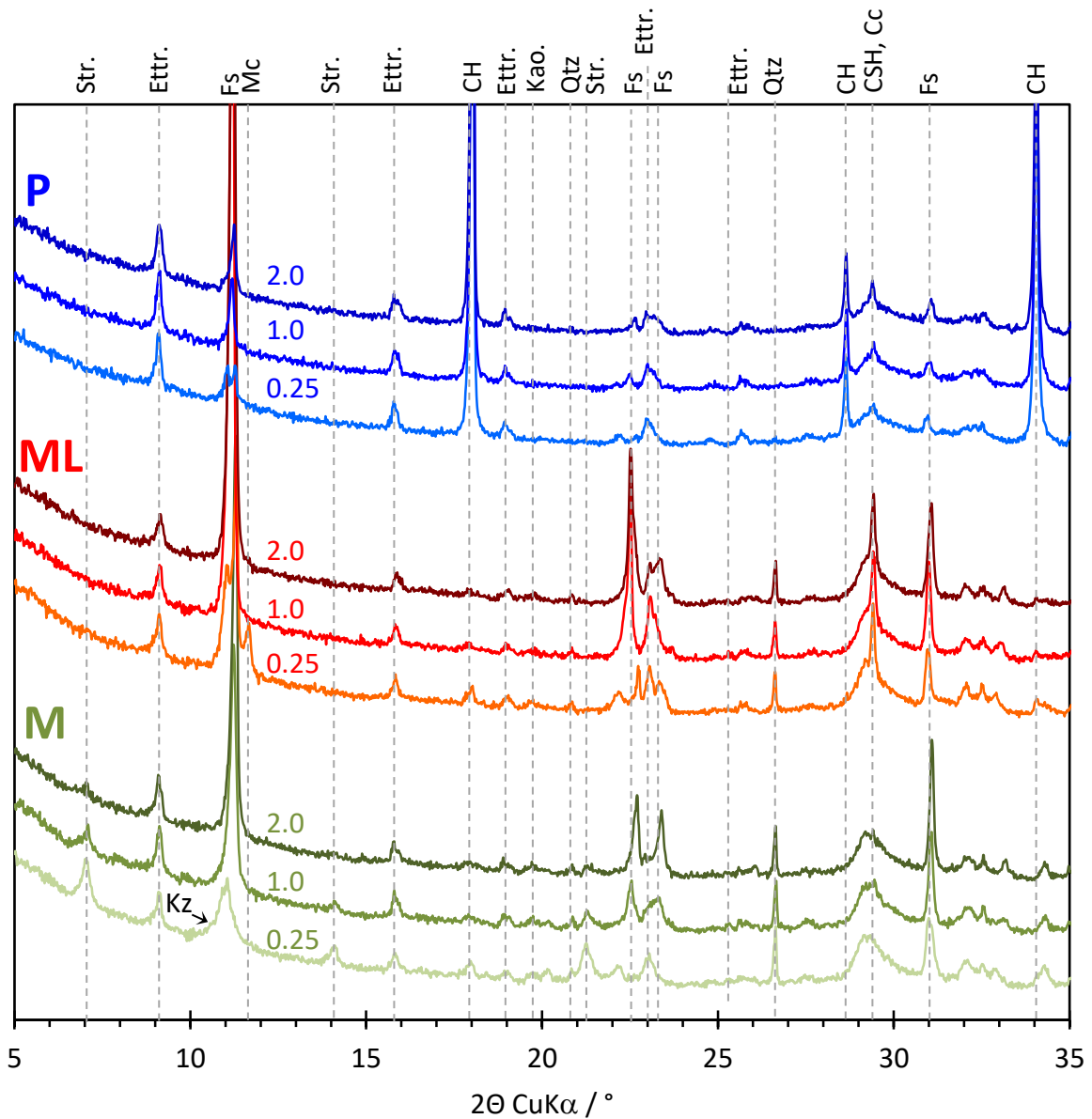
787



788

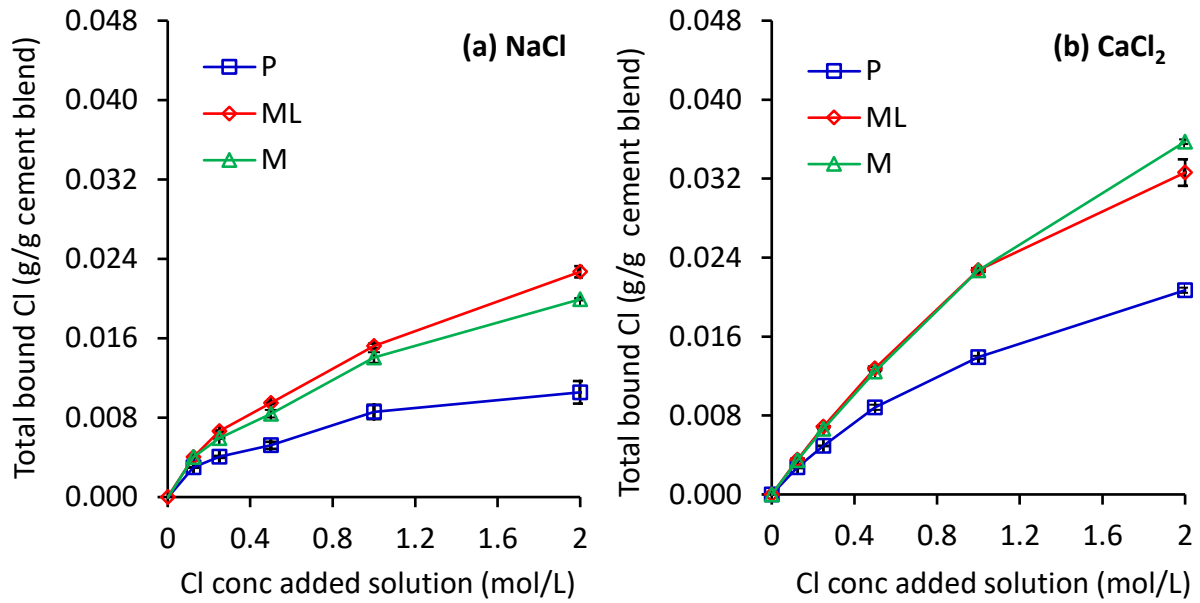


789 **Fig. 2.** DTG curves of the pastes exposed to the NaCl (a, c and e) and CaCl₂ (b, d and f)
 790 solutions with different chloride concentrations (0 - 2.0 mol/L). The area of the second weight
 791 loss for Friedel's salt is highlighted. CSH: calcium-silicate-hydrate; Ettr.: ettringite; Fs:
 792 Friedel's salt; Mc: monocarbonate; Str: strätlingite; CH: portlandite; Cc: calcium carbonate
 793

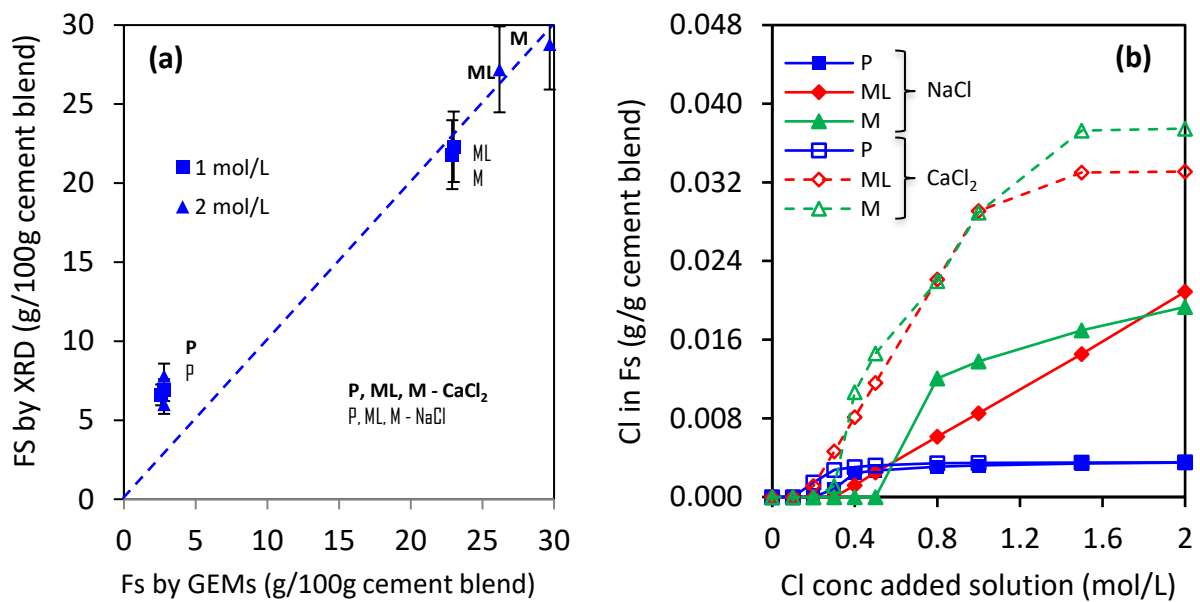


794
 795 **Fig. 3.** XRD patterns of the pastes exposed to the CaCl_2 solutions with different chloride
 796 concentration (0.25, 1.0 and 2.0 mol/L). CSH: calcium-silicate-hydrate; Ettr.: ettringite; Fs:
 797 Friedel's salt; Mc: monocarbonate; Str: strätlingite; CH: portlandite; Cc: calcium carbonate; Kz:
 798 Kuzel's salt; Kao.: Kaolinite; Qtz.: Quartz.

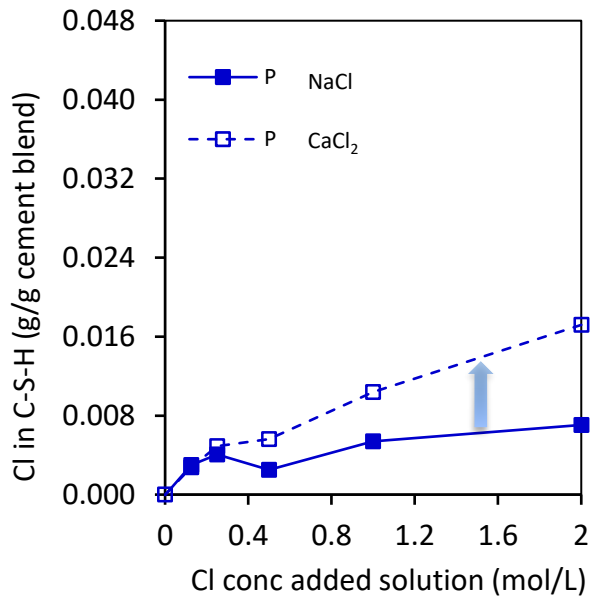
799
 800
 801



802
 803 **Fig. 4.** Chloride binding isotherms for the P, ML and M pastes exposed to (a) NaCl and (b)
 804 CaCl₂ solutions. The bound chloride content is reported as g per g of unhydrated cement blend
 805 and shown as a function of the concentration of added chloride ions in the exposure solutions.
 806
 807

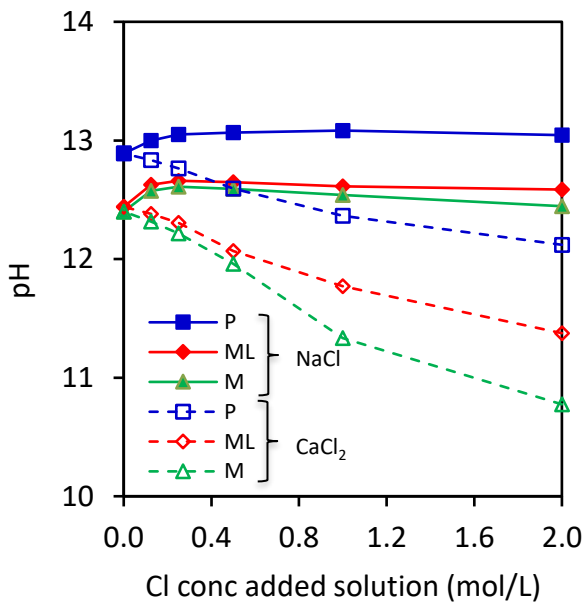


808
 809 **Fig. 5.** Chloride bound as Friedel's salt for all the pastes exposed to the NaCl and CaCl₂
 810 solutions. (a) Relationship between the calculated (by thermodynamic modeling) and measured
 811 (by XRD) amount of Friedel's salt. (b) The amount of chloride binding isotherm from Friedel's
 812 salt predicted by thermodynamic modeling.
 813



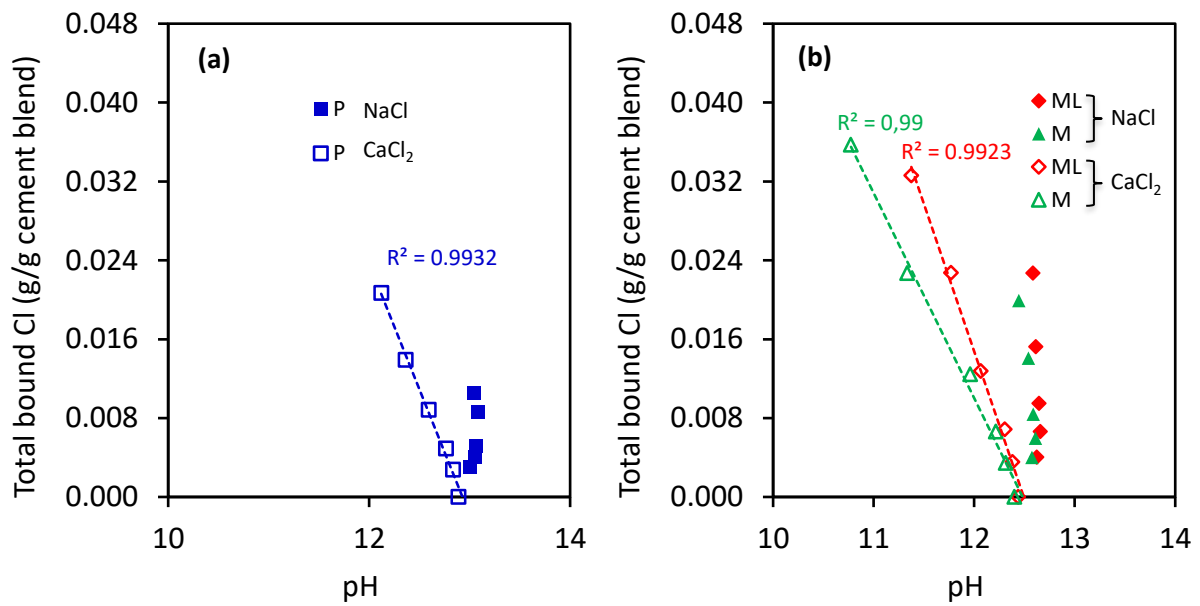
814
815
816 **Fig. 6.** Chloride absorbed on the C-S-H phase in the P pastes calculated by subtracting the
817 bound chloride in Friedel's salt predicted by thermodynamic modeling from the total bound
818 chloride.

819
820



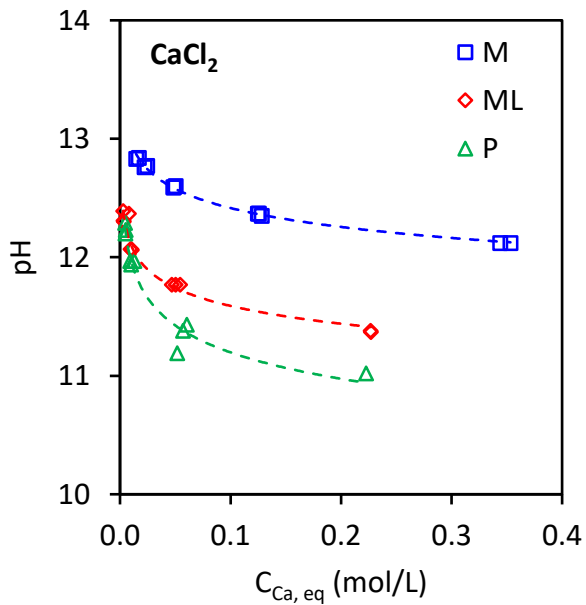
821
822
823 **Fig. 7.** pH values as a function of the chloride concentrations of the exposure solutions for the
824 pastes exposed to the NaCl and CaCl₂ solutions.

825
826



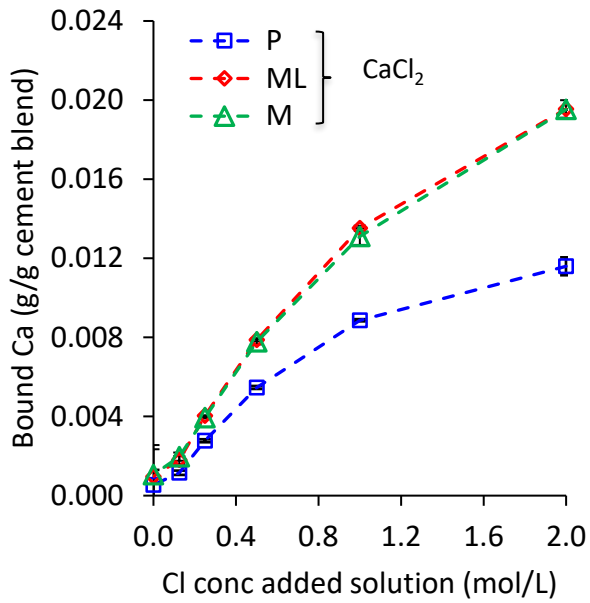
827
 828 **Fig. 8.** Relationship between the total bound chloride and the pH of the exposure solutions for
 829 (a) the P paste and (b) the ML and M pastes exposed to the NaCl and CaCl₂ solutions.

830
 831



832
 833 **Fig. 9.** Relationship between pH and the measured calcium concentration ($C_{Ca,eq}$) in the CaCl₂
 834 exposure solution at equilibrium condition.

835
 836



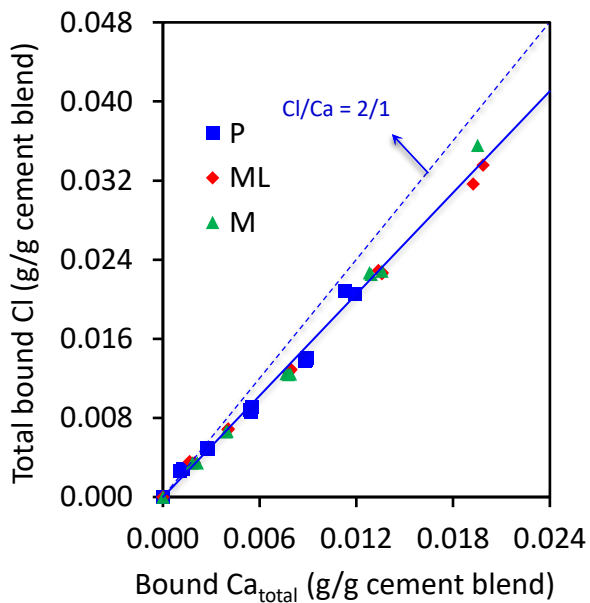
837

838

839 **Fig. 10.** Calcium binding isotherm (*i.e.*, uptake of calcium from the CaCl_2 exposure solution by
 840 hydration products) for the well-hydrated P, ML and M pastes exposed to the CaCl_2 solution.

841

842



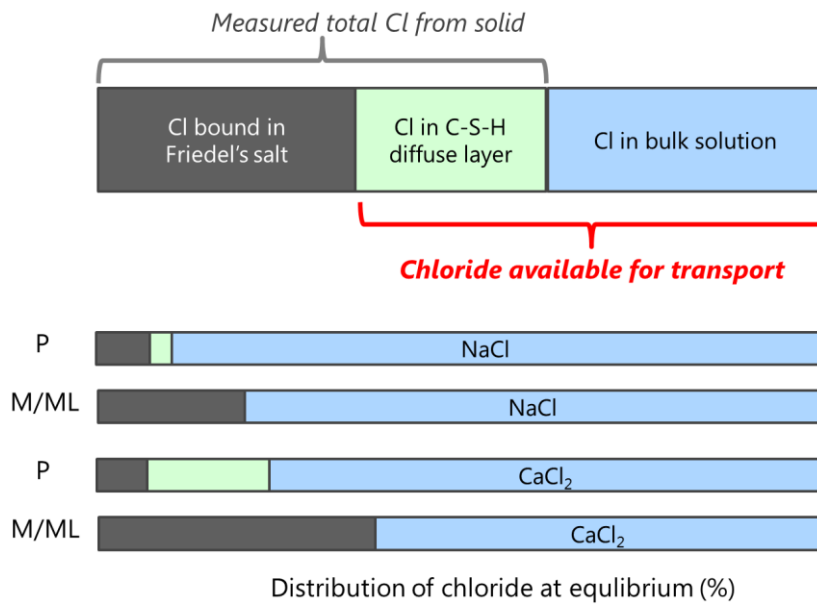
843

844

845 **Fig. 11.** Relationship between the total bound chloride and the total “bound” calcium (*i.e.*,
 846 uptake of calcium from the CaCl_2 exposure solution by hydration products) for pastes exposed
 847 to the CaCl_2 solution for pastes exposed to the CaCl_2 solution.

848

849



850
 851 **Fig. 12.** Schematic description of the chloride distribution in the P, ML and M paste samples
 852 exposed to the NaCl and CaCl₂ solutions.
 853